JACS
JOURNAL OF THE AMERICAN CHEMICAL SOCIETY
pubs.acs.org/JACS
Article

Thermoelectric–Photoelectrochemical Water Splitting under Concentrated Solar Irradiation

Chanon Pornrungroj,[‡] Virgil Andrei,[‡] and Erwin Reisner*

Cite This: https://doi.org/10.1021/jacs.3c01892
Read Online

ABSTRACT: Photoelectrochemical devices could play a crucial role toward fuel production in a circular economy. Yet, light absorption suffers losses from thermalization and the inability to use low-energy photons. Here, we demonstrate that photoelectrochemical reactors can utilize this waste heat by integrating thermoelectric modules, which provide additional voltage under concentrated light irradiation. While most single semiconductors require external bias, we already accomplish unassisted water splitting under 2 sun irradiation by wiring a $BiVO_4$ photoanode to a thermoelectric element, whereas the photocurrent of a perovskite-$BiVO_4$ tandem system is enhanced 1.7-fold at 5 sun. This strategy is particularly suitable for photoanodes with more positive onset potentials like hematite, with thermoelectric-perovskite-Fe_2O_3 systems achieving a 29.7× overall photocurrent increase at 5 sun over conventional perovskite-Fe_2O_3 devices without light concentration. This thermal management approach provides a universal strategy to facilitate widespread solar fuel production, as light concentration increases output, reduces the reactor size and cost, and may enhance catalysis.

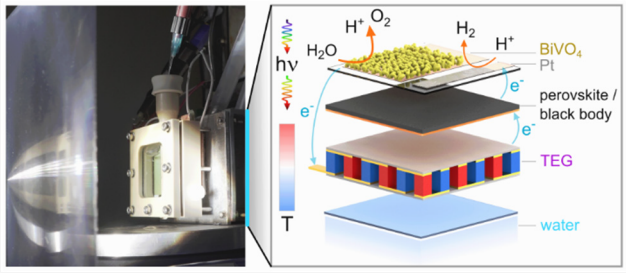

INTRODUCTION

A broad utilization of the solar spectrum is key for efficient solar fuel production.[1,2] Yet, light absorbers are limited by the maximum achievable efficiency known as the Shockley–Queisser limit.[3] Hence, over 50% of the total energy is lost through thermalization or from nonabsorbed visible and IR photons with energies below the semiconductor bandgap.[1,3] The resulting heating is known to decrease the photovoltage and promote photovoltaic (PV) cell degradation.[4] However, higher temperatures can also prove beneficial by accelerating the reaction rate of electrocatalysis in solar fuel production.[4] Strategies such as up- and downconversion have been employed to overcome this limitation, but challenges remain in the overall system integration and material stability under ambient conditions.[5−7]

A complementary route to harvest this waste heat is presented by thermoelectrics (TEs).[2] In this case, a potential difference is induced along a material in the presence of a temperature gradient, which is known as the Seebeck effect.[8−10] An array of such p- and n-type doped semiconductors can be assembled electrically in series and thermally in parallel to form a thermoelectric generator (TEG, see scheme in Figure S1).[8] Its additional Seebeck voltage can be particularly useful in aiding photoelectrochemical (PEC) fuel production, as the thermodynamic requirements, catalyst overpotentials, and band positions of conventional photoelectrodes make overall water splitting challenging.

While a number of solar concentrator TE[11,12] and TE-PV[13,14] systems prove the utility of this approach for electricity production, few reports proposed TE systems for solar fuel synthesis.[2,15,16] However, earlier TE-PEC studies only investigated photoelectrodes under 1 sun irradiation, meaning that the temperature difference (ΔT) was controlled by active heating requiring an external energy input. Accordingly, a decoupled TE-Si-Pt design needed an externally set ΔT above 60 K to overcome >2 V for overall water splitting,[16] whereas a more integrated TE-Si-$BiVO_4$ system only attained a light-induced ΔT of 9 K due to its side-on irradiation.[15]

Here, we introduce an integrated TE-PEC design for overall water splitting under concentrated solar irradiation. This design makes use of the entire spectral range, by placing the single or tandem light absorbers and heat-harvesting TEG in a single optical light path (Figure 1a,b). In this case, a steady temperature gradient is sustained via passive heating, by conveniently placing the commercial TEG between a hot PEC reactor and a room-temperature water bath emulating the open water sources (e.g., lakes, rivers) used in industrial cooling (Figure 1). This setup benefits from the higher temperatures attained under light concentration, as unassisted water splitting is already achieved when interfacing a commercial TEG with a

Received: February 20, 2023

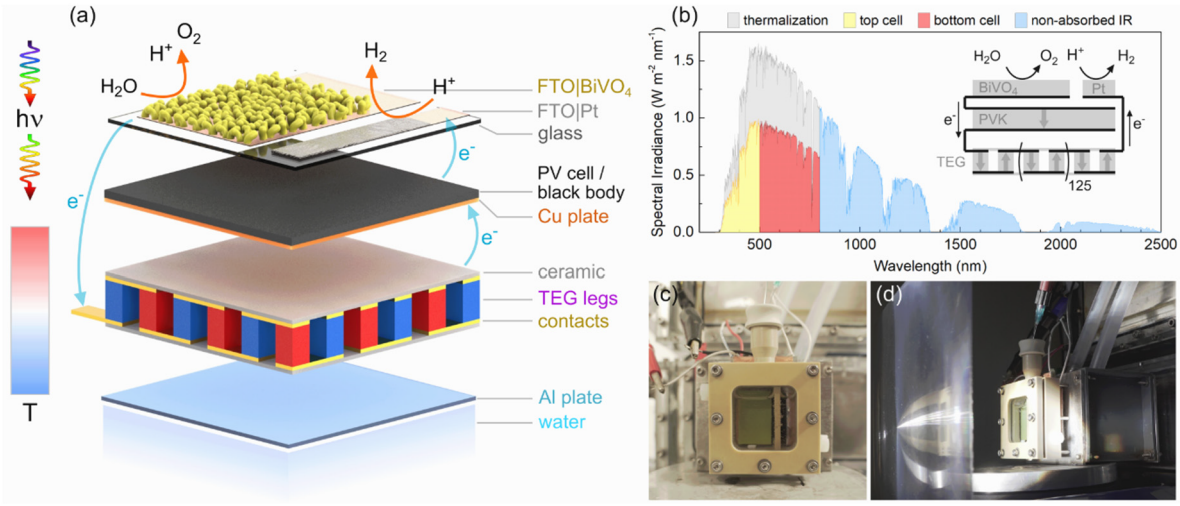

Figure 1. Architecture of the integrated thermoelectric−photoelectrochemical setup for solar water splitting. (a) Expanded schematic of the device assembly. The $BiVO_4$ photoanode and Pt cathode are deposited on patterned FTO glass. Higher wavelength light is transmitted to either a perovskite PV cell or a blackbody converting light into heat. This temperature difference between the light absorbers and water bath is harvested by a TEG to provide additional voltage. (b) Solar spectrum (ASTM G173-03 AM1.5G reference spectrum) utilization by a tandem light harvesting device. Incident energy is lost as waste heat from thermalization or nonabsorbed photons (simplified schematic is plotted assuming 60% EQE for both light absorbers). The inset depicts the wiring of an integrated TE-PEC device. The $BiVO_4$ photoanode, perovskite cell, and Pt cathode are wired electrically in series to a commercial TEG, which is comprised of 127 TE leg pairs. (c, d) Photographs of the assembled reactor without irradiation (c) and operating under concentrated light irradiation (d). A separator is mounted between the $BiVO_4$ and Pt electrodes (c). The Fresnel lens and rear water bath help sustain the temperature difference (d).

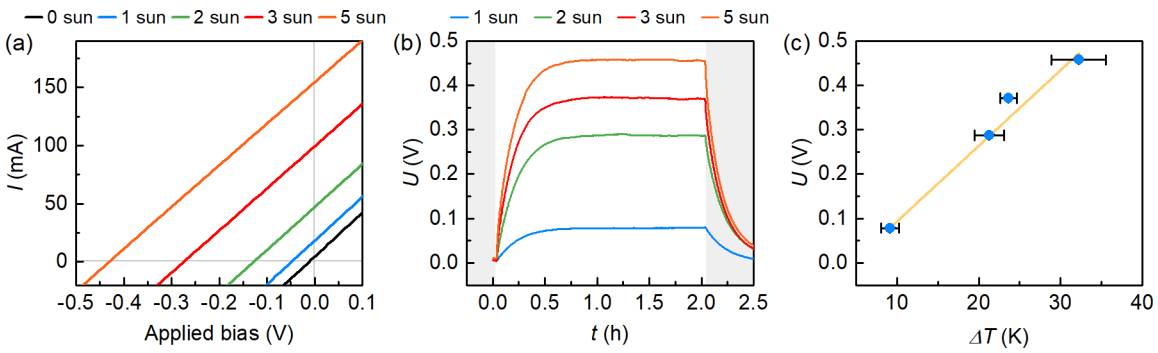

Figure 2. Voltage output of a TEG caused by reactor heating under light concentration. (a) Averaged $I-V$ curves of a TE module under 1−5 sun irradiation (forward and backward scans are given in Figure S14). (b) Chronopotentiometry of the corresponding TEG under open-circuit conditions. The TEG is integrated in a Pt-TE-$BiVO_4$ assembly to emulate the heating behavior observed under operation. (c) Linear relationship between the Seebeck voltage (U) and the temperature difference (see values in Table S1).

single light absorber, a $BiVO_4$ photoanode. A broadband coverage of the solar spectrum, from UV to the IR range, is demonstrated when introducing an additional perovskite (PVK) PV cell between the $BiVO_4$ and TE components. The applicability of this thermal management strategy to various light absorbers is exemplified using hematite (α-Fe_2O_3), as TE-PVK-Fe_2O_3 assemblies display a significant photocurrent increase under light concentration despite the lower hematite photovoltage. This truly integrated circuit makes use of charge, photon, and heat flows, demonstrating the potential of overall energy management.

■ RESULTS AND DISCUSSION

TEG-Photoanode Integration. The energy levels required for overall water splitting limit the choice of materials to a small selection of wide bandgap semiconductors. To demonstrate the benefits of our heat harvesting concept, we first assembled a TE-PEC system containing a single light absorber. For this purpose, we chose a robust $BiVO_4$ photoanode, which displays high photocurrents reaching 3 mA cm^{-2} and an early onset potential of 0.2 V against the reversible hydrogen electrode (RHE) for oxygen evolution.[17] The photoanode was wired to a commercial TEG (Kimilar Peltier Cooler, TEC1-12706, 40 × 40 × 4 mm^3, proprietary TE legs), to demonstrate the versatility of our approach. A custom setup was designed to induce a temperature difference between the two sides of a TEG (Figure 1, Figures S2−S4). Accordingly, the TEG was sandwiched between a PEC front reactor and a 3D-printed water bath acting as the heat sink, with thermal grease enabling appropriate heat transfer (Figure S3a−c). A small volume of the PEC reactor ensured a relatively rapid heating of the electrolyte solution (13.5 mL) under concentrated irradiation, whereas effective cooling was achieved by taking advantage of the high thermal conductivity of water (∼24 times higher compared to air).[18] Variable solar concentration was achieved using a Fresnel lens, with the light

https://doi.org/10.1021/jacs.3c01892
J. Am. Chem. Soc. XXXX, XXX, XXX−XXX

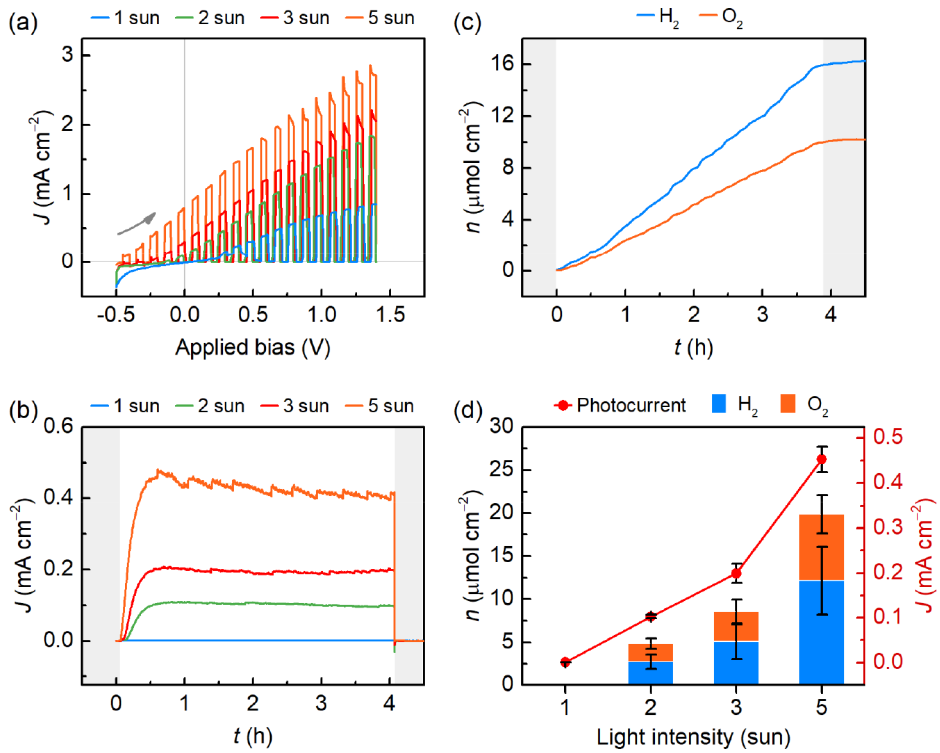

Figure 3. Performance of a Pt-TE-$BiVO_4$ system for overall solar water splitting. (a) Chopped-light LSV of the integrated Pt-TE-$BiVO_4$ system under different light intensities. (b) Representative CPE traces of bias-free water splitting under 1−5 sun irradiation. (c) Example of product evolution during 4 h CPE (Pt-TE-$BiVO_4$, 5 sun). Products are quantified by gas chromatography under N_2 flow, by sampling from the reactor headspace every 4.25 min (see Methods in Supporting Information). (d) Average steady-state photocurrents and corresponding product amounts over 4 h CPE under varying light concentration. Experiments were performed in a 0.1 M KB_i, 0.1 M K_2SO_4 electrolyte solution (pH 8.5, temperature 34−61 °C), whereas the water bath was maintained at 25 °C. Gray shades indicate no irradiation.

intensity calibrated to 1−5 sun (100−500 mW cm^{-2}) with an optical power meter (details in Supporting Information).

In this configuration, a patterned glass slide containing two FTO stripes acts as the back window of the PEC reactor (Figure 1a,c, Figure S5a). A 6 cm^2 $BiVO_4$ photoanode with a spin-coated TiCo O_2 evolution catalyst (OEC) was deposited on one stripe following reported procedures,[19,20] whereas Pt was selectively sputtered as the H_2 evolution catalyst (HEC) on the second FTO stripe (see Methods in Supporting Information). The two side-by-side electrodes operated in a 0.1 M potassium borate buffer (KB_i) solution of pH 8.5, with aqueous 0.1 M K_2SO_4 as electrolyte solution. The $BiVO_4$ photoanode utilized short-wavelength light for oxygen evolution (<500 nm),[20] whereas longer wavelength photons (>500 nm) were converted to heat using a matte black absorbing layer on the rear side of the glass substrate (Figures S6 and S7a,c,d). The formation of the $BiVO_4$ nanoporous structure was further confirmed by scanning electron microscopy (SEM) images and X-ray diffraction (XRD) of the electrode (Figures S8a and S9).

The $BiVO_4$ photoanode maintained an onset voltage of ∼0.2 V for water splitting against the Pt cathode (Pt-$BiVO_4$) under concentrated light irradiation (Figure S10), whereas the electrolyte temperature reached ∼60 °C under 5 sun irradiation (Figure S11 and Table S1). While an increase in the electrolyte temperature does not significantly affect catalysis (see controls in Figures S12 and S13), the resulting temperature difference could be utilized by the TE module to provide an additional voltage of 17.1 ± 1.0 mV K^{-1}. The Seebeck voltage increased linearly with the temperature difference reaching 0.46 V under open-circuit conditions, under a ΔT of 32.2 ± 3.3 K at 5 sun irradiation (Figure 2, Figure S14, and Table S1). Accordingly, the linear sweep voltammetry (LSV) traces of the integrated Pt-TE-$BiVO_4$ system could be shifted negatively by up to ∼0.5 V under 5 sun irradiation, enabling unassisted water splitting at light intensities as low as 2 sun (Figure 3a and Figure S15).

These findings were confirmed by controlled potential electrolysis (CPE) measurements at zero applied bias voltage. The photocurrent densities stabilized within the first hour of irradiation following the change in the Seebeck voltage, as the temperature gradient reached steady state (Figures 2b and 3b). Accordingly, a photocurrent of 0.10 ± 0.01 mA cm^{-2} was observed under 2 sun irradiation, which could be further increased to 0.45 ± 0.03 mA cm^{-2} under 5 sun illumination (Figure 3b). The latter corresponded to a solar-to-hydrogen (STH) efficiency of 0.11%, which compares well among most single light absorber systems reported for overall water splitting (see Tables S2 and S3).[21] A similar trend was observed in the product amounts, reaching 12.16 ± 3.94 μmol cm^{-2} H_2 and 7.72 ± 2.24 μmol cm^{-2} O_2 over 4 h of CPE under 5 sun (Figure 3c,d), whereas no products could be detected in the absence of the TE module. A deviation in the H_2:O_2 ratio from 2:1 was observed for most samples (Figure 3c) and can be attributed to bubble trapping and calibration limitations at low O_2 amounts.

TEG Integration with Perovskite-$BiVO_4$ Tandem Devices. The TE element was further integrated into a perovskite-$BiVO_4$ tandem structure[17,19] to assess its potential toward enhancing the performance of established solar fuel

https://doi.org/10.1021/jacs.3c01892
J. Am. Chem. Soc. XXXX, XXX, XXX−XXX

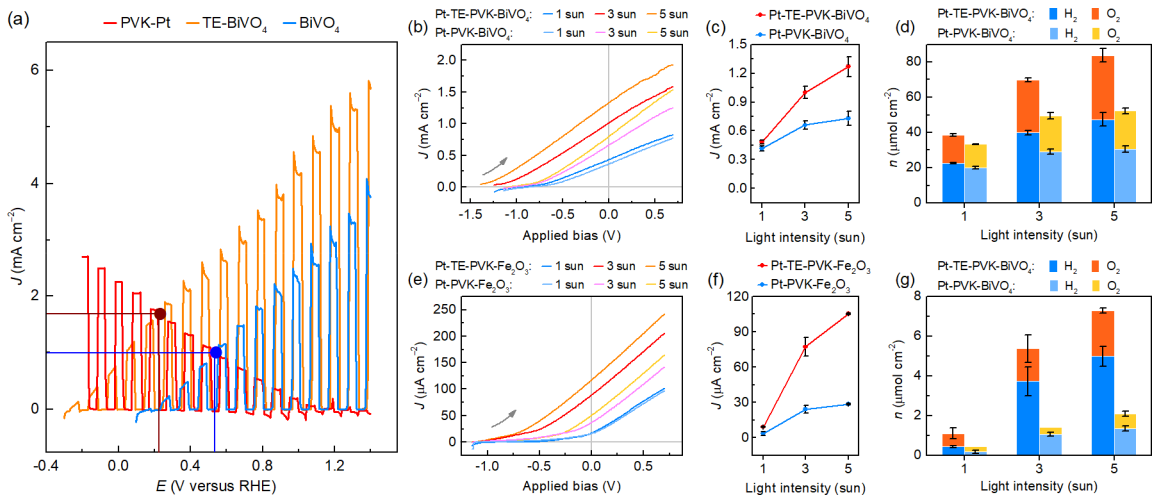

Figure 4. TE integration enhances the performance of PVK-oxide tandem devices for solar water splitting. (a) Intersection of LSV curves recorded for PVK-Pt, TE-$BiVO_4$, and $BiVO_4$ in a three-electrode setup under 5 sun irradiation. (b−d) Performance of Pt-PVK-$BiVO_4$ tandem devices with or without an integrated TEG under varying light concentration. (e−g) Corresponding data for Pt-PVK-Fe_2O_3 and Pt-TE-PVK-Fe_2O_3 assemblies. (b, e) LSV traces. (c, f) Steady-state photocurrents for unassisted water splitting. (d, g) Product amounts obtained after 4 h of CPE at 0 V applied bias. Experiments were performed in 0.1 M KB_i, 0.1 M K_2SO_4 buffer, pH 8.5 for $BiVO_4$ and in 1 M NaOH when using a Fe_2O_3 photoanode (34−61 °C solution temperature; 25 °C water bath temperature).

systems. For this purpose, a triple cation mixed halide perovskite solar cell (abbreviated PVK) was sandwiched between the $BiVO_4$ photoanode and the TEG (Figure 1a). The 6 cm^2 PV cell was wired in series with both items, providing an additional photovoltage of ∼1.05 V, as shown from the histograms and $J-V$ curves in Figures S16 and S17. The solar cell was encapsulated with a hydrophobic graphite epoxy paste covered by a flat copper foil to ensure a good thermal contact with the TEG underneath (Figure S18).

The operating parameters of an unassisted PEC tandem device can be estimated from the overlap of the LSV curves for both photoelectrodes.[1] The corresponding photocurrent density (J_{op}) and applied potential (V_{op}) help predict the product rates and selectivity, which become key in cases when a high overpotential must be overcome, for instance in unassisted CO_2 reduction.[22] The integrated TE element holds promise to improve both parameters, by shifting the intersection point of the two electrodes. To illustrate this, we plotted the LSV curves of the $BiVO_4$ photoanode wired to the TEG (TE-$BiVO_4$) and of the perovskite PV cell wired to the Pt cathode (PVK-Pt, equivalent to our buried PV photocathodes[17,19]), which were determined in a three-electrode configuration with a Ag/AgCl reference and Pt counter electrode. LSV curves recorded under 1 and 5 sun irradiation displayed indeed that not only is the J_{op} expected to be improved, but also the V_{op} could be altered (Figure 4a and Figure S19).

LSV curves of the full Pt-TE-PVK-$BiVO_4$ system confirmed the beneficial effect of TEG integration, which became again more significant under elevated light flux. In this case, the photocurrent matching between the $BiVO_4$ and PVK-Pt elements governs the overall tandem performance. Both light absorbers attain matching photocurrent densities of a few mA cm^{-2} (Figure 4a), which overlap at an absolute photocurrent of around 6 mA under 5 sun illumination (Figure S19c). In contrast, the TE element can operate at currents above 100 mA under a similar light concentration, due to its minimal electrical resistance of 2.6 Ω (see $I-V$ curves in Figure 2a). As a result, the operating conditions of the serially connected Pt-TE-PVK-$BiVO_4$ system are close to the open-circuit voltage of the TE element, maximizing the applied TE voltage without affecting the overall photocurrent (Figure S19c).[23] Accordingly, a ∼0.5 V negative shift could be again observed under 5 sun irradiation, resulting in a notable improvement in the onset voltage of approximately −1.4 V for overall water splitting (Figure 4b). Under these conditions, the Pt-TE-PVK-$BiVO_4$ system reached a steady-state photocurrent of 1.27 ± 0.10 mA cm^{-2} (STH of 0.31 ± 0.13%) yielding the highest improvement, 1.7 times, over the 0.73 ± 0.08 mA cm^{-2} photocurrent of a classical PVK-$BiVO_4$ tandem device (Figure 4c, Figure S20a, Tables S4 and S5). Similar trends were observed in the amounts of products, amounting to a total of 47.5 ± 3.8 μmol cm^{-2} H_2 and 36.3 ± 3.6 μmol cm^{-2} O_2 for the Pt-TE-PVK-$BiVO_4$ system (4 h CPE, 5 sun; Figure 4d and Figure S20b).

Scope of the Thermoelectric Integration. While the early onset potential of $BiVO_4$ toward O_2 evolution makes it an excellent photoanode material for tandem PEC devices, the onset potentials of other established light absorbers (e.g., WO_3, or hematite) restrict the choice of photocathodes for overall water splitting. Thermoelectric integration has the potential to overcome these limitations, by providing the additional voltage required for unassisted water splitting.

To demonstrate the versatility of our concept to a broad scope of tandem configurations, we therefore replaced $BiVO_4$ with an α-Fe_2O_3 photoanode. Although hematite is an earth abundant photoanode material with a favorable optical bandgap (2.2 eV) and good stability under deleterious chemical conditions, it suffers from poor charge transport and short excited-state lifetime,[24] resulting in an onset potential of only 0.8 V vs RHE for O_2 evolution (Figure S21). Here, 6 cm^2 α-Fe_2O_3 photoanodes were fabricated on FTO-coated glass substrates via a previously reported hydrothermal method.[25] Photoanodes showed an absorption edge around 600 nm and a deep red color (Figure S6 and S7b). SEM and XRD confirmed the formation of porous α-Fe_2O_3 photoanodes (Figures S8b and S9).

The heat-induced ∼0.5 V shift in the onset voltage (Figure 4e) was especially beneficial for the Pt-TE-PVK-Fe_2O_3 system,

https://doi.org/10.1021/jacs.3c01892
J. Am. Chem. Soc. XXXX, XXX, XXX−XXX

as PVK-Pt and α-Fe_2O_3 electrodes only display a limited LSV overlap (Figure S22).[26,27] The average steady-state photocurrents amounted to 9.08 ± 0.54 and 105.4 ± 0.7 μA cm^{-2} for Pt-TE-PVK-Fe_2O_3 devices, whereas Pt-PVK-Fe_2O_3 only reached 3.55 ± 1.64 and 28.5 ± 0.7 μA cm^{-2} under 1 and 5 sun, respectively. Accordingly, the TE integration yielded a 3.7 times photocurrent improvement under 5 sun, which is significantly higher than the 1.7× improvement attained in the corresponding Pt-TE-PVK-$BiVO_4$ arrangement (Figure 4f, Figure S23a, Tables S6 and S7). More importantly, this represents a 29.7× improvement for Pt-TE-PVK-Fe_2O_3 at 5 sun over the photocurrent of Pt-PVK-Fe_2O_3 tandem devices under 1 sun irradiation, highlighting the beneficial complementary effects of light concentration and thermoelectric waste heat harvesting. The photocurrents began to plateau under stronger light irradiation for both $BiVO_4$ and Fe_2O_3 systems, following the conventional $J-V$ shape of PV and PEC components. The same trends were observed in the product evolution, amounting to 4.99 ± 0.50 μmol cm^{-2} H_2 and 2.30 ± 0.11 μmol cm^{-2} O_2 for Pt-TE-PVK-Fe_2O_3 over 4 h of CPE under 5 sun (Figure 4g and Figure S23b).

While differences in light concentration, photovoltages, and catalytic overpotentials prevent a direct correlation between the efficiency of the individual components and their assembly, these results indicate that an additional Seebeck voltage is key to enable overall solar fuel production in PEC systems with insufficient photovoltage, such as Pt-$BiVO_4$ or Pt-PVK-Fe_2O_3. The additional voltage provided by the TE element may allow such PEC tandems to overcome the high overpotentials associated with other demanding reactions including CO_2 reduction[22] and N_2 fixation, whereas the increased temperature may further improve reaction kinetics.[4,28] In addition, thermal integration may prevent overheating or temperature fluctuations, which would avoid the degradation and photovoltage losses encountered in classical PV-electrolysis systems.

In an industrial context where the total output becomes more relevant than device efficiency, this technology could provide significant benefits in terms of costs and material consumption,[29,30] as large-area devices may be replaced by small reactors coupled to relatively inexpensive plastic Fresnel lenses. Accordingly, light concentration would offset the cost of adding an additional TE module, making such integrated circuits more commercially competitive. As great emphasis has been recently placed on the advantages of light concentration and thermal management,[4,31] our approach may provide a route to improve the performance of such upscaled systems. However, further design improvements are still needed with respect to heat transfer, thermal insulation, or controlled electrolyte flow to prevent overheating.[4,28] Metal fingers will also be required to mitigate resistive losses on a large scale, as in-plane parasitic effects are already noticeable in the case of our 6 cm^2 light absorbers, limiting photocurrent densities below those of small-scale tandem PV-PEC devices.[32]

CONCLUSIONS

This work demonstrates that direct waste heat utilization can benefit PEC devices, as the additional thermoelectric bias voltage increases product output and device photocurrent. A steady temperature difference is maintained via passive heating across the two sides of a commercial TE module, by integrating either single or tandem light absorbers with the TEG in a single optical light path. This thermal management approach enables unassisted overall water splitting even for PEC systems with insufficient photovoltage. Accordingly, overall water splitting is achieved with a single $BiVO_4$ photoanode and a Pt cathode at light intensities as low as 2 sun, whereas the ~0.5 V shift in the onset voltage induces a 3.7× photocurrent enhancement under 5 sun for a perovskite-Fe_2O_3 tandem. This integrated energy harvesting system makes use of charge, light, and heat flows, providing a proof-of-concept for scalable, overall energy management.

ASSOCIATED CONTENT

Supporting Information

The Supporting Information is available free of charge at https://pubs.acs.org/doi/10.1021/jacs.3c01892.

Experimental details, synthesis procedures, device assembly and characterization, supplementary tables, and supplementary data figures (PDF)

AUTHOR INFORMATION

Corresponding Author

Erwin Reisner − *Yusuf Hamied Department of Chemistry, University of Cambridge, Cambridge CB2 1EW, United Kingdom*; orcid.org/0000-0002-7781-1616; Email: reisner@ch.cam.ac.uk; http://www-reisner.ch.cam.ac.uk

Authors

Chanon Pornrungroj − *Yusuf Hamied Department of Chemistry, University of Cambridge, Cambridge CB2 1EW, United Kingdom*; orcid.org/0000-0001-9886-8489

Virgil Andrei − *Yusuf Hamied Department of Chemistry, University of Cambridge, Cambridge CB2 1EW, United Kingdom*; orcid.org/0000-0002-6914-4841

Complete contact information is available at: https://pubs.acs.org/10.1021/jacs.3c01892

Author Contributions

‡C.P. and V.A. contributed equally. C.P., V.A., and E.R. conceived the idea and designed the project. C.P. prepared the photoelectrodes and conducted physical characterization of the semiconductors. V.A. prepared perovskite devices. C.P. performed the photoelectrochemical experiments. V.A. carried out H_2 and O_2 quantification. C.P. and V.A. drafted and E.R. edited the manuscript. All authors contributed to data analysis, discussion, and completion of the manuscript. E.R. supervised the work.

Notes

The authors declare no competing financial interest.

ACKNOWLEDGMENTS

This work was supported by the Cambridge Trust (Cambridge Thai Foundation Award to C.P.), a Trinity-Henry Barlow Scholarship (to C.P.), the Cambridge Philosophical Society (to C.P.), the Winton Programme for the Physics of Sustainability and St John's College Cambridge (Title A Research Fellowship to V.A.), and a European Research Council (ERC) Consolidator Grant (MatEnSAP, 682833, to E.R.). We are thankful to Dr. Motiar Rahaman and Dr. Yongpeng Liu (University of Cambridge) for useful feedback on the manuscript.

REFERENCES

(1) Wang, Q.; Pornrungroj, C.; Linley, S.; Reisner, E. Strategies to improve light utilization in solar fuel synthesis. *Nat. Energy* **2022**, *7*, 13−24.

(2) Andrei, V.; Bethke, K.; Rademann, K. Thermoelectricity in the context of renewable energy sources: joining forces instead of competing. *Energy Environ. Sci.* **2016**, *9*, 1528−1532.

(3) Shockley, W.; Queisser, H. J. Detailed balance limit of efficiency of p−n junction solar cells. *J. Appl. Phys.* **1961**, *32*, 510−519.

(4) Tembhurne, S.; Nandjou, F.; Haussener, S. A thermally synergistic photo-electrochemical hydrogen generator operating under concentrated solar irradiation. *Nat. Energy* **2019**, *4*, 399−407.

(5) Choi, D.; Nam, S. K.; Kim, K.; Moon, J. H. Enhanced photoelectrochemical water splitting through bismuth vanadate with a photon upconversion luminescent reflector. *Angew. Chem., Int. Ed.* **2019**, *58*, 6891−6895.

(6) Trupke, T.; Green, M.; Würfel, P. Improving solar cell efficiencies by up-conversion of sub-band-gap light. *J. Appl. Phys.* **2002**, *92*, 4117−4122.

(7) Zhang, M.; Lin, Y.; Mullen, T. J.; Lin, W.-f.; Sun, L.-D.; Yan, C.-H.; Patten, T. E.; Wang, D.; Liu, G.-y. Improving hematite's solar water splitting efficiency by incorporating rare-earth upconversion nanomaterials. *J. Phys. Chem. Lett.* **2012**, *3*, 3188−3192.

(8) Snyder, G. J.; Toberer, E. S. Complex thermoelectric materials. *Nat. Mater.* **2008**, *7*, 105−114.

(9) Biswas, K.; He, J.; Blum, I. D.; Wu, C.-I.; Hogan, T. P.; Seidman, D. N.; Dravid, V. P.; Kanatzidis, M. G. High-performance bulk thermoelectrics with all-scale hierarchical architectures. *Nature* **2012**, *489*, 414−418.

(10) Borup, K. A.; de Boor, J.; Wang, H.; Drymiotis, F.; Gascoin, F.; Shi, X.; Chen, L.; Fedorov, M. I.; Müller, E.; Iversen, B. B.; Snyder, G. J. Measuring thermoelectric transport properties of materials. *Energy Environ. Sci.* **2015**, *8*, 423−435.

(11) Kraemer, D.; Poudel, B.; Feng, H.-P.; Caylor, J. C.; Yu, B.; Yan, X.; Ma, Y.; Wang, X.; Wang, D.; Muto, A.; McEnaney, K.; Chiesa, M.; Ren, Z.; Chen, G. High-performance flat-panel solar thermoelectric generators with high thermal concentration. *Nat. Mater.* **2011**, *10*, 532−538.

(12) Kraemer, D.; Jie, Q.; McEnaney, K.; Cao, F.; Liu, W.; Weinstein, L. A.; Loomis, J.; Ren, Z.; Chen, G. Concentrating solar thermoelectric generators with a peak efficiency of 7.4%. *Nat. Energy* **2016**, *1*, 16153.

(13) Charalambous, P. G.; Maidment, G. G.; Kalogirou, S. A.; Yiakoumetti, K. Photovoltaic thermal (PV/T) collectors: A review. *Appl. Therm. Eng.* **2007**, *27*, 275−286.

(14) Van Sark, W.G.J.H.M. Feasibility of photovoltaic−thermoelectric hybrid modules. *Appl. Energy* **2011**, *88*, 2785−2790.

(15) Kang, Y.; Chen, R.; Zhen, C.; Wang, L.; Liu, G.; Cheng, H.-M. An integrated thermoelectric-assisted photoelectrochemical system to boost water splitting. *Sci. Bull.* **2020**, *65*, 1163−1169.

(16) Jung, J.-Y.; Woong Kim, D.; Kim, D.-H.; Joo Park, T.; Wehrspohn, R. B.; Lee, J.-H. Seebeck-voltage-triggered self-biased photoelectrochemical water splitting using HfO_x/SiO_x bi-layer protected Si photocathodes. *Sci. Rep.* **2019**, *9*, 9132.

(17) Pornrungroj, C.; Andrei, V.; Rahaman, M.; Uswachoke, C.; Joyce, H. J.; Wright, D. S.; Reisner, E. Bifunctional perovskite−$BiVO_4$ tandem devices for uninterrupted solar and electrocatalytic water splitting cycles. *Adv. Funct. Mater.* **2021**, *31*, 2008182.

(18) Ramires, M. L.; Nieto de Castro, C. A.; Nagasaka, Y.; Nagashima, A.; Assael, M. J.; Wakeham, W. A. Standard reference data for the thermal conductivity of water. *J. Phys. Chem. Ref. Data* **1995**, *24*, 1377−1381.

(19) Andrei, V.; Hoye, R. L. Z.; Crespo-Quesada, M.; Bajada, M.; Ahmad, S.; De Volder, M.; Friend, R.; Reisner, E. Scalable triple cation mixed halide perovskite−$BiVO_4$ tandems for bias-free water splitting. *Adv. Energy Mater.* **2018**, *8*, 1801403.

(20) Kim, T. W.; Choi, K.-S. Nanoporous $BiVO_4$ photoanodes with dual-layer oxygen evolution catalysts for solar water splitting. *Science* **2014**, *343*, 990−994.

(21) Wang, Q.; Nakabayashi, M.; Hisatomi, T.; Sun, S.; Akiyama, S.; Wang, Z.; Pan, Z.; Xiao, X.; Watanabe, T.; Yamada, T.; Shibata, N.; Takata, T.; Domen, K. Oxysulfide photocatalyst for visible-light-driven overall water splitting. *Nat. Mater.* **2019**, *18*, 827−832.

(22) Andrei, V.; Reuillard, B.; Reisner, E. Bias-free solar syngas production by integrating a molecular cobalt catalyst with perovskite−$BiVO_4$ tandems. *Nat. Mater.* **2020**, *19*, 189−194.

(23) Park, K.-T.; Shin, S.-M.; Tazebay, A. S.; Um, H.-D.; Jung, J.-Y.; Jee, S.-W.; Oh, M.-W.; Park, S.-D.; Yoo, B.; Yu, C.; Lee, J.-H. Lossless hybridization between photovoltaic and thermoelectric devices. *Sci. Rep.* **2013**, *3*, 2123.

(24) Mesa, C. A.; Francàs, L.; Yang, K. R.; Garrido-Barros, P.; Pastor, E.; Ma, Y.; Kafizas, A.; Rosser, T. E.; Mayer, M. T.; Reisner, E.; Grätzel, M.; Batista, V. S.; Durrant, J. R. Multihole water oxidation catalysis on haematite photoanodes revealed by operando spectroelectrochemistry and DFT. *Nat. Chem.* **2020**, *12*, 82−89.

(25) Xiao, J.; Huang, H.; Huang, Q.; Li, X.; Hou, X.; Zhao, L.; Ma, R.; Chen, H.; Li, Y. Remarkable improvement of the turn−on characteristics of a Fe_2O_3 photoanode for photoelectrochemical water splitting with coating a FeCoW oxy−hydroxide gel. *Appl. Catal., B* **2017**, *212*, 89−96.

(26) Sharma, P.; Jang, J. W.; Lee, J. S. Key strategies to advance the photoelectrochemical water splitting performance of α-Fe_2O_3 photoanode. *ChemCatChem.* **2019**, *11*, 157−179.

(27) Li, F.; Jian, J.; Xu, Y.; Wang, S.; Wang, H.; Wang, H. Recent advances on interfacial engineering of hematite photoanodes for viable photo-electrochemical water splitting. *Eng. Rep.* **2021**, *3*, e12387.

(28) Yang, L.; Chen, Z. G.; Dargusch, M. S.; Zou, J. High performance thermoelectric materials: progress and their applications. *Adv. Energy Mater.* **2018**, *8*, 1701797.

(29) Andrei, V.; Ucoski, G. M.; Pornrungroj, C.; Uswachoke, C.; Wang, Q.; Achilleos, D. S.; Kasap, H.; Sokol, K. P.; Jagt, R. A.; Lu, H.; Lawson, T.; Wagner, A.; Pike, S. D.; Wright, D. S.; Hoye, R. L. Z.; MacManus-Driscoll, J. L.; Joyce, H. J.; Friend, R. H.; Reisner, E. Floating perovskite-$BiVO_4$ devices for scalable solar fuel production. *Nature* **2022**, *608*, 518−522.

(30) Sokol, K. P.; Andrei, V. Automated synthesis and characterization techniques for solar fuel production. *Nat. Rev. Mater.* **2022**, *7*, 251−253.

(31) Dumortier, M.; Haussener, S. Design guidelines for concentrated photo-electrochemical water splitting devices based on energy and greenhouse gas yield ratios. *Energy Environ. Sci.* **2015**, *8*, 3069−3082.

(32) Kim, J. H.; Jo, Y.; Kim, J. H.; Jang, J. W.; Kang, H. J.; Lee, Y. H.; Kim, D. S.; Jun, Y.; Lee, J. S. Wireless solar water splitting device with robust cobalt-catalyzed, dual-doped $BiVO_4$ photoanode and perovskite solar cell in tandem: a dual absorber artificial leaf. *ACS Nano* **2015**, *9*, 11820−11829.

https://doi.org/10.1021/jacs.3c01892
J. Am. Chem. Soc. XXXX, XXX, XXX−XXX